Surface Chemistry for Atomic Layer Growth

S. M. George,* A. W. Ott, and J. W. Klaus

Department of Chemistry and Biochemistry, University of Colorado, Boulder, Colorado 80309-0215

Received: December 12, 1995; In Final Form: May 8, 1996[⊗]

Atomic layer controlled film growth is an important technological and scientific goal that is closely tied to many issues in surface chemistry. This article first reviews the basic concepts of atomic layer growth using molecular precursors and binary reaction sequence chemistry. Many examples are given for the various films that have been grown using this atomic layer growth technique. The paradigms for atomic layer epitaxy (ALE) and atomic layer processing (ALP) are then discussed in terms of self-limiting surface reactions. Recent investigations of the surface chemistry of SiO_2 and Al_2O_3 ALP and GaAs ALE are examined and used to illustrate the possible mechanisms of atomic layer growth. Subsequently, the characteristics of film deposition using atomic layer growth techniques are explored using recent examples for Al_2O_3 ALP. The structure of the deposited films is also reviewed using results from previous Al_2O_3 deposition investigations. This article then concludes by discussing possible complications to studies of atomic layer controlled growth using binary reaction sequence chemistry.

I. Introduction

Atomic layer control of growth is an ultimate goal of nanofabrication technology. Control of deposition at the atomic scale will be necessary in electronic devices in the very near future.[1−4] For example, the SiO_2 gate oxides in MOSFET devices are already approaching 50−60 Å thicknesses and will probably be pushed to ∼30 Å thicknesses before this insulating SiO_2 layer reaches the tunneling limit. These ultrathin SiO_2 film thicknesses represent only ∼10 atomic layers.

Various approaches have been explored to obtain atomic layer controlled growth. One of the most straightforward is molecular beam epitaxy (MBE) where an elemental beam is impinged on the surface to deposit a very well-defined amount of atoms. The deposition is controlled by knowing the atomic flux and exposing the surface to this flux for a certain time. Another approach is to utilize molecular precursors to transport the elements to the substrate. There are many advantages to using molecular precursors that include higher vapor pressures compared with elemental sources and deposition that does not require line of sight to the sample.

One important feature of molecular precursors is that they can provide atomic layer control of deposition. This control can be inherent in the self-limiting surface chemistry that occurs during the deposition. This molecular precursor approach was originally pioneered by T. Suntola and co-workers in Finland for the atomic layer epitaxy (ALE) of ZnS.[5−8] Subsequent research by Nishizawa and others developed similar ALE strategies for GaAs deposition.[9,10] During the past 15 years, there has been a rapid expansion of the ALE approach for the deposition of a variety of thin films. Much of the early work was summarized in the review by Goodman and Pessa.[5]

More recent ALE investigations have continued to expand the number of films that can be deposited with atomic layer control. In many cases, these films are not epitaxial, and the deposition should probably be referred to as atomic layer processing (ALP) instead of ALE. Whatever the name, the basic ALE strategy involves self-limiting surface reactions that provide the atomic layer control of growth. This paper will review this important molecular precursor approach to thin film deposition and focus on the basic surface chemistry that underlies the ALE strategy. Although the deposition of a variety of different films has been demonstrated, understanding the basic surface chemistry has not received much attention.

The surface chemistry underlying the ALP approaches may also affect the characteristics of the deposited film. Recent work has begun to explore the surface morphology of deposited films with atomic force microscopy (AFM).[11−14] There is early evidence that the details of the surface chemistry may play an important role in dictating the film quality, surface morphology, and surface roughness. Understanding the nature of ALP deposition and its correlation with the underlying surface chemistry may provide important new challenges and opportunities for surface scientists.

II. Basic Concepts of Atomic Layer Controlled Growth

The basic concepts that define the ALE or ALP molecular precursor approach are based on self-limiting surface reactions. In general, the ALE approach is most appropriate for binary compounds because a binary chemical vapor deposition reaction can easily be separated into two half-reactions. Using ZnS deposition as a model example, the overall binary reaction for ZnS thin film growth is $ZnCl_2 + H_2S \rightarrow ZnS + 2HCl$.[6−8] This binary reaction can be divided into the two model half-reactions:

$$\text{(A)}\quad ZnCl^* + H_2S \rightarrow ZnSH^* + HCl$$

$$\text{(B)}\quad SH^* + ZnCl_2 \rightarrow SZnCl^* + HCl$$

where the asterisks designate the surface species. The (A) half-reaction exposes the surface to the H_2S molecular precursor only, deposits sulfur, and converts the chlorinated surface to a hydride surface. The zinc is deposited in the (B) half-reaction by exposure to only the $ZnCl_2$ molecular precursor, and this reaction converts the hydride surface back to the chlorinated surface. This general AB binary reaction sequence is shown schematically in Figure 1.

Following the (B) half-reaction, the surface is back in the original state and is ready for another (A) half-reaction. As a result, the repetition of the half-reactions in an ABAB... sequence will lead to the deposition of sulfur and zinc in an atomic layer-by-layer fashion. The repetitive ABAB... sequence of these half-reactions can be described as binary reaction sequence chemistry.[15−17] The simple model for binary reaction sequence chemistry assumes that the surface has a finite number of reactive chemical groups. The half-reactions will proceed until all the starting reactive functional groups (e.g., ZnCl*) have

* To whom correspondence should be addressed.

[⊗] Abstract published in *Advance ACS Abstracts,* July 1, 1996.

S0022-3654(95)03676-8 CCC: $12.00

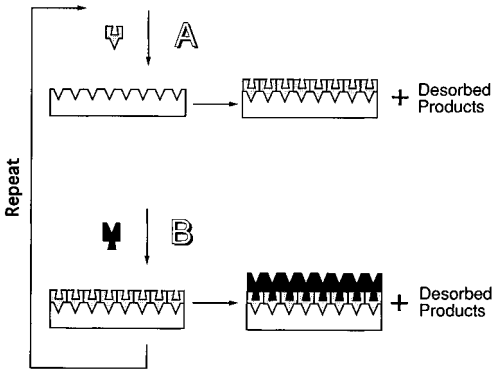

Figure 1. Schematic representation of atomic layer controlled deposition using self-limiting surface chemistry and an AB binary reaction sequence.

been converted into the other functional group (e.g., ZnSH*). At this point, the surface reaction will limit itself because there are no more reactive sites for additional deposition.

During each half-reaction, the surface functionality changes from one surface species to another (e.g., ZnCl* → SH* → ZnCl* → SH*). This model assumes a direct substitution reaction between the molecular precursor and the surface species. The direct one-for-one substitution leads to a finite coverage that can be deposited during each half-reaction. This picture for the ALE approach also predicts that the amount of deposition per half-reaction will be dependent on the coverage of the surface functional groups. Consequently, the thermal stability of the surface functional groups should be an important factor in determining the film growth per AB reaction cycle.

An alternative model for binary reaction sequence chemistry is that the molecular precursors transport the elements to the surface, but the ligands on the elements desorb during or soon after the half-reaction. In this case, the atomic layer control of growth occurs because the first monolayer is chemically bound much more tightly than successive monolayers. If the molecular precursors cannot easily dissociatively chemisorb after the first monolayer has been deposited or if the surface temperature is high enough to desorb the successive monolayers, then atomic layer control can be achieved without direct substitution reactions. This model for ALP is similar to the original ALE approach for the deposition of ZnS using elemental sources.[7]

Although the basic ALE approach is most easily applied to binary compounds, ALE schemes have also been devised for single element film growth. In this case the atomic layer control is obtained by surface species that inhibit deposition. The ABAB... binary reaction sequence approach for the atomic layer growth of single elements involves a molecular precursor deposition step (A) and subsequent adsorbate removal (B). The adsorbate removal step may involve a temperature jump or exposure to a second species, such as atoms, electrons, or ions, that initiates the adsorbate desorption.

These models for binary reaction sequence chemistry are the limiting cases, and the actual mechanism may be much more complex. Because the surface chemistry has only been explored in a few instances, the actual mechanisms are not clearly understood and may involve combinations of the simple models described above. Other factors may also affect the mechanism such as steric hindrance between the surface species and geometrical difficulties in obtaining the epitaxial monolayer growth of crystalline materials. There also may be Langmuir−Hinshelwood reactions between surface species in addition to the direct substitution reactions between the molecular precursor and the surface adsorbates.

III. Films Grown Using Binary Reaction Sequence Chemistry

Since the original demonstration of the ALE molecular precursor approach for ZnS deposition, many additional binary reactions have been utilized in an ABAB... binary reaction sequence to deposit films with atomic layer control. The initial work by Suntola and co-workers focused on ZnS and other II/VI materials because of their importance in electroluminescent devices.[7,18] Additional semiconductor and oxide systems have subsequently been explored for a variety of applications in electroluminescent displays, semiconductor devices, and multilayer structures. In addition, the conformal growth resulting from the self-limiting nature of the ALP surface chemistry is important for uniform deposition on high aspect ratio structures and porous materials.[11,19]

Many of the binary chemical vapor deposition reactions that have been split into two separate half-reactions are listed in Scheme 1. Although the reactions are balanced according to

Scheme 1

II/VI Compounds

ZnS: $ZnCl_2 + H_2S \rightarrow ZnS + 2HCl$ [6-8]

CdTe: $Cd(CH_3)_2 + Te(C_3H_7)_2 \rightarrow CdTe + 2C_4H_{10}$ [20]

III/V Compounds

GaAs: $Ga(CH_3)_3 + AsH_3 \rightarrow GaAs + 3CH_4$ [9, 10]

GaN: $Ga(CH_3)_3 + NH_3 \rightarrow GaN + 3CH_4$ [21, 22]

Oxide Compounds

SiO_2: $SiCl_4 + 2H_2O \rightarrow SiO_2 + 4HCl$ [15, 17]

Al_2O_3: $2Al(CH_3)_3 + 3H_2O \rightarrow Al_2O_3 + 6CH_4$ [11, 15, 16, 23, 24]

SnO_2: $SnCl_4 + 2H_2O \rightarrow SnO_2 + 4HCl$ [25]

TiO_2: $TiCl_4 + 2H_2O \rightarrow TiO_2 + 4HCl$ [12, 19, 26, 27]

ZrO_2: $ZrCl_4 + 2H_2O \rightarrow ZrO_2 + 4HCl$ [13]

In_2O_3: $2InCl_3 + 3H_2O \rightarrow In_2O_3 + 6HCl$ [28]

HfO_2: $HfCl_4 + 2H_2O \rightarrow HfO_2 + 4HCl$ [29]

Nitride and Sulfide Compounds

Si_3N_4: $3SiCl_4 + 4NH_3 \rightarrow Si_3N_4 + 12HCl$ [30]

AlN: $Al(CH_3)_3 + NH_3 \rightarrow AlN + 3CH_4$ [31]

In_2S_3: $2InCl_3 + 3H_2S \rightarrow In_2S_3 + 6HCl$ [32-34]

Elemental Deposition

Si: $H_2Si(CH_2CH_3)_2 + \Delta T \rightarrow Si + CH_2{=}CH_2 + 2H_2$ [33, 34]

$Si_2Cl_6 + Si_2H_6 \rightarrow Si + 6HCl$ [35]

Ge: $H_2Ge(CH_2CH_3)_2 + \Delta T \rightarrow Ge + CH_2{=}CH_2 + 2H_2$ [36-38]

proper stoichiometry, the balanced reactions do not necessarily imply that the actual surface chemistry leads to these particular reaction products. The reaction products are given assuming a direct substitution model for the binary reaction sequence

chemistry. The reaction products will be very different if the surface functional groups or ligands desorb during or soon after the half-reaction.

IV. Surface Chemistry Underlying Atomic Layer Growth

Very few studies have focused on the surface chemistry during ALE or ALP film growth.[15,17,24,27,38−40] The notable exception is the ALE deposition of GaAs, which has been explored by numerous investigators.[39,40] Additional systems that have received more attention recently are the ALP deposition of SiO_2[15,17] and Al_2O_3.[15,16] The surface chemistry that occurs during ALE or ALP has not been examined for most of the other systems listed in Section III.

One reason for the paucity of surface chemistry studies is that most ALP reactions are carried out in flow reactors or require high pressures. The flow reactors are not generally built with *in situ* surface probes. In addition, many surface science techniques require an ultrahigh-vacuum (UHV) environment and are not applicable at the higher required pressures for many surface reactions. UHV chambers can be equipped with separate isolatable chambers that avoid contamination of the main UHV chamber during high-pressure exposures.[41] One such chamber was recently employed to investigate the surface chemistry of SiO_2 ALP on Si(100).[17,41]

Another method of surface analysis that does not require an UHV environment and can monitor surface species is transmission FTIR spectroscopy.[16,17,24,27] However, high surface area substrates are often required because of the small cross section of infrared vibrational transitions. This method has been employed recently in studies of the surface chemistry of SiO_2 ALP on oxidized porous silicon substrates[15,17] and Al_2O_3 ALP on alumina membranes.[15,16] The previous studies of SiO_2 and Al_2O_3 ALP will be discussed first before reviewing the more complicated results for GaAs ALE.

A. SiO_2 and Al_2O_3 Atomic Layer Processing. The binary reaction sequence proposed for SiO_2 ALP is as follows:[17]

$$\text{(A)}\quad \mathrm{SiOH^*} + \mathrm{SiCl_4} \rightarrow \mathrm{Si{-}O{-}SiCl_3^*} + \mathrm{HCl}$$

$$\text{(B)}\quad \mathrm{SiCl^*} + \mathrm{H_2O} \rightarrow \mathrm{SiOH^*} + \mathrm{HCl}$$

where the surface species are marked with asterisks. All the surface species shown above have vibrational stretches that are infrared-active. Consequently, transmission FTIR studies can be used to investigate the surface reactions and determine whether the reactions are self-limiting.

Figure 2 shows two regions of the IR spectrum as a function of $SiCl_4$ exposure during the (A) reaction on an hydroxylated oxidized porous silicon surface.[17] The initial hydroxylated surface begins with a single feature at ∼3740 cm^{-1} that is consistent with SiOH* surface species. As the surface is exposed to $SiCl_4$ at 10 Torr and 600 K, the hydroxyl feature at 3740 cm^{-1} decreases and a new feature at ∼625 cm^{-1} appears that is assigned to Si−Cl stretching vibrations. The loss of the hydroxyl feature coincides with the growth of the silicon chloride feature. Figure 3 displays the corresponding IR spectrum as a function of H_2O exposure during the (B) reaction.[17]

Figure 4 shows the integrated absorbances for the features at ∼3740 and ∼625 cm^{-1} during the (A) and (B) reactions.[17] Both reactions were carried out at 600 K and 10 Torr. These IR results are consistent with the proposed reactions given above. In the (A) reaction, SiOH* species are completely replaced with $SiCl_x$* species versus $SiCl_4$ exposure. In the (B) reaction, the $SiCl_x$* species are completely replaced by SiOH* versus H_2O exposure. For both reactions, the loss of the initial surface functional group is concurrent with the gain of the resulting functional group.[17] Each reaction is self-limiting and terminates with the consumption of the initial functional group.

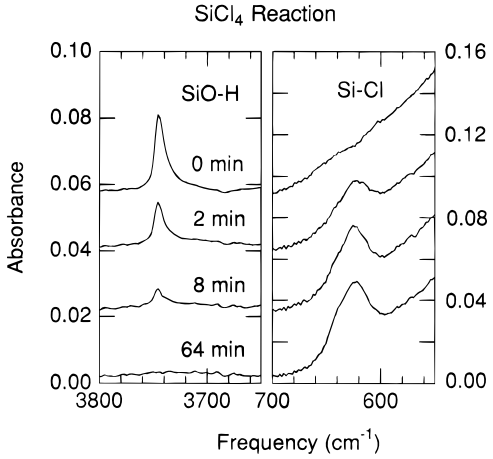

Figure 2. FTIR spectra during the $SiCl_4$ reaction at 600 K and 10 Torr on a hydroxylated oxidized porous silicon surface. The reduction of the SiO−H stretching vibration at ∼3740 cm^{-1} is concurrent with the growth of the Si−Cl stretching vibration at ∼625 cm^{-1}.

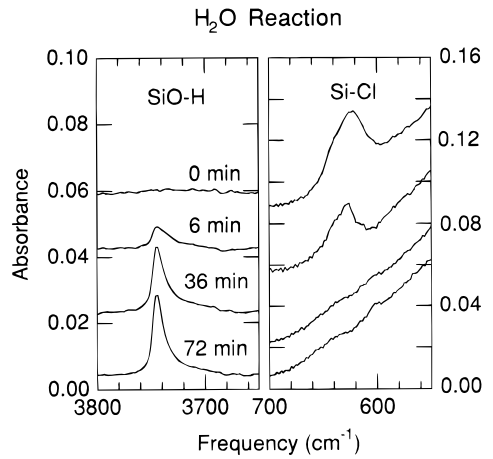

Figure 3. FTIR spectra during the H_2O reaction at 600 K and 10 Torr on the chlorine-terminated surface produced by the $SiCl_4$ reaction. The reduction of the Si−Cl stretching vibration at ∼625 cm^{-1} is concurrent with the growth of the SiO−H stretching vibration at ∼3740 cm^{-1}.

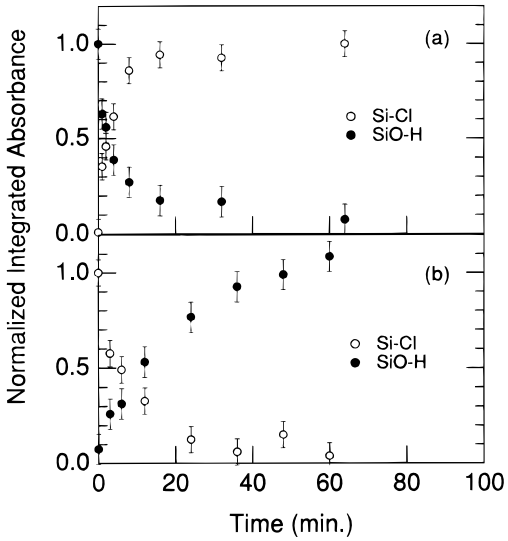

Figure 4. Integrated absorbances of the Si−Cl stretching vibration at ∼625 cm^{-1} and the SiO−H stretching vibration at ∼3740 cm^{-1} as a function of time during the (a) $SiCl_4$ and (b) H_2O half-reactions at 600 K and 10 Torr.

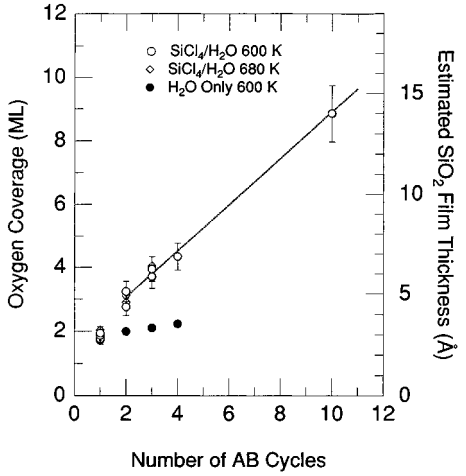

Figure 5. Oxygen coverage and SiO_2 film thickness as a function of the number of AB cycles. The oxygen coverage from only H_2O thermal oxidation is shown for comparison.

Although high surface area samples are useful for transmission FTIR studies, they cannot easily determine the deposition rate per AB reaction cycle. For these measurements, the (A) and (B) reactions were performed on a single-crystal Si(100) surface using an UHV chamber equipped with an internal high-pressure cell.[17,41] The growth of SiO_2 was monitored by the SiO temperature-programmed desorption from the SiO_2 layer after various numbers of AB reaction cycles. The oxygen coverages versus number of AB reaction cycles determined by this method are shown in Figure 5.[17] These measurements were consistent with a growth rate of ~1.1 Å/AB cycle. Figure 5 also displays results for only H_2O exposures that indicate that both $SiCl_4$ and H_2O are necessary for SiO_2 film growth at this temperature.

Another binary reaction sequence that has been extensively studied using FTIR spectroscopy is Al_2O_3 growth using trimethylaluminum (TMA) and water. The proposed set of half-reactions for this deposition sequence is[16,23]

$$\text{(A)}\quad \mathrm{AlOH^* + Al(CH_3)_3 \rightarrow Al{-}O{-}Al(CH_3)_2^* + CH_4}$$

$$\text{(B)}\quad \mathrm{AlCH_3^* + H_2O \rightarrow AlOH^* + CH_4}$$

where again the asterisks indicate surface species. Early studies probed the surface species with FTIR and Auger electron spectroscopic techniques and were consistent with the above mechanism.[24]

More detailed studies of these binary reactions were also performed using transmission FTIR spectroscopy on high surface area alumina membranes.[16] In these studies, the AlOH* surface species were monitored using the hydroxyl (O−H) vibrational stretching feature that has a broad peak at ~3500 cm^{-1}. The hydroxyl feature is significantly broadened because of extensive hydrogen bonding. The $AlCH_3$* surface species were monitored using the sharper methyl (C−H) vibrational stretching feature that is centered near ~2900 cm^{-1}. This FTIR study showed that while the (A) reaction does occur at room temperature, the reaction does not go to completion at any exposure time or pressure.[16]

Figure 6 shows two complete reaction cycles using 0.3 Torr, 1 min reactant exposures at 500 K.[16] After each TMA dose, the broad hydroxyl feature is completely replaced by the methyl feature at ~2900 cm^{-1}. The hydroxyl feature returns to its original size, and the methyl feature completely disappears after the H_2O exposure. These infrared spectra show that both the (A) and (B) binary reactions are complete and self-limiting at this temperature and exposure.[16]

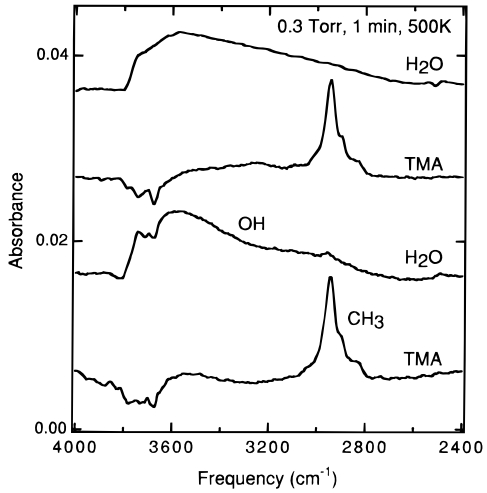

Figure 6. Infrared absorption spectra of porous alumina membranes versus sequential 0.3 Torr, 1 min H_2O and TMA exposures at 500 K.

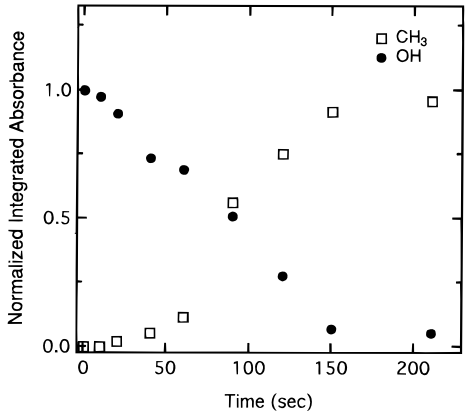

Figure 7. Normalized integrated absorbances of the AlO−H and AlC−H_3 stretching vibrations versus time during a 0.01 Torr of TMA exposure on porous alumina membranes at 500 K. The reduction of the AlO−H stretching vibration at ~3500 cm^{-1} is concurrent with the growth of the AlC−H stretching vibration at ~2900 cm^{-1}.

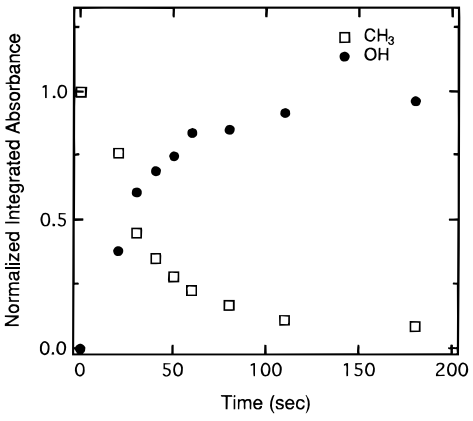

Figure 8. Normalized integrated absorbances of the AlO−H and AlC−H_3 stretching vibrations versus time during a 0.01 Torr of H_2O exposure on porous alumina membranes at 500 K. The reduction of the AlC−H stretching vibration at ~2900 cm^{-1} is concurrent with the growth of the AlO−H stretching vibration at ~3500 cm^{-1}.

Figures 7 and 8 show the integrated absorbances for the hydroxyl groups (O−H stretching vibration) and methyl groups (C−H stretching vibration) during the (A) and (B) reactions versus time for exposures of 0.01 Torr at 500 K.[16] These results provide information about the nature of these reactions. The absorbance from the C−H stretching vibration saturates when the absorbance from the O−H stretching vibration reaches zero for the (A) reaction. The reverse is also true for the (B) reaction.

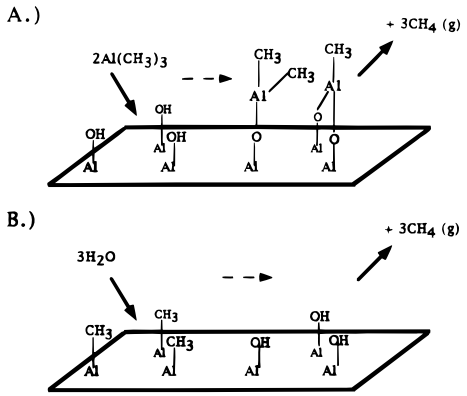

Figure 9. Possible mechanisms for the surface chemistry of Al_2O_3 controlled deposition using TMA and H_2O in a binary reaction sequence.

This behavior is consistent with self-limiting surface reactions and supports the proposed reaction mechanism given above and illustrated in Figure 9.[16]

More information can be obtained by looking in detail at the early stages of the (A) reaction. Figure 7 shows that the hydroxyl coverage decreases initially while there is very little increase in the methyl coverage.[16] This observation is consistent with one TMA molecule reacting with more than one hydroxyl site early in the (A) reaction. As the hydroxyl coverage is decreased, TMA molecules can no longer react with more than one hydroxyl group, and the hydroxyl loss and methyl gain are more concurrent.[16] On the other hand, there is a coincident increase in the hydroxyl coverage and decrease in the methyl coverage at all times during the (B) reaction as displayed in Figure 8. This correlation is consistent with each H_2O molecule reacting with one CH_3 group.[16] These FTIR spectra are very convincing that Al_2O_3 ALP is dominated by self-limiting surface chemistry.

B. GaAs Atomic Layer Epitaxy. The ALE growth of GaAs is one of the few systems where the surface chemistry has been studied in tandem with the film growth. The large interest in GaAs ALE is motivated by the desire to develop higher speed devices with optoelectronic capabilities.[42] Nishizawa and co-workers were the first to demonstrate GaAs ALE at low pressures using trimethylgallium (TMGa) and arsine (AsH_3).[9,10] They observed ALE deposition of GaAs over a limited temperature and pressure range.

Ozeki et al. have also produced exciting GaAs ALE results by demonstrating a wide range of experimental parameters for ALE growth.[43] The range of conditions where ALE will occur is commonly called the "ALE window". Their reported ALE window includes pressures from 10^{-5} to 10^{-1} Torr, temperatures ranging from 450 to 550 °C, and pulse durations from 1 to 25 s. These experimental results might suggest that GaAs ALE proceeds by a similar ligand exchange mechanism that is observed in SiO_2 and Al_2O_3 ALP.[15] A direct surface exchange mechanism for the GaAs binary reaction sequence chemistry may be

$$\text{(A)}\quad \text{AsH}^* + \text{Ga(CH}_3)_3 \rightarrow \text{AsGa(CH}_3)_2^* + \text{CH}_4$$

$$\text{(B)}\quad \text{Ga(CH}_3)^* + \text{AsH}_3 \rightarrow \text{GaAsH}_2^* + \text{CH}_4$$

Unfortunately, the surface chemistry of GaAs is much more complex than this simple proposed binary reaction sequence. There is strong evidence against the direct substitution reactions that were described above for SiO_2 and Al_2O_3 ALP. At GaAs ALE growth temperatures, some of the CH_3 groups are known to desorb as methyl radicals, and surface hydrogen can desorb as H_2. A schematic representation of the surface chemistry that may be more consistent with the experimental results is

$$\text{(A)}\quad \text{As}^* + \text{Ga(CH}_3)_3 \rightarrow \text{AsGa(CH}_3)^* + 2(^{\bullet}\text{CH}_3)$$

$$\text{(B)}\quad \text{Ga(CH}_3)^* + \text{AsH}_3 \rightarrow \text{GaAs}^* + \text{CH}_4 + \text{H}_2$$

where the • denotes a radical species. This schematic is also an oversimplification of the complex surface chemistry that occurs during GaAs ALE as will be explained further below.

The three different mechanisms of GaAs ALE that have received the most attention are the selective adsorption, adsorbate inhibition, and the flux balance models. The selective adsorption mechanism[44,45] assumes that TMGa converts an arsenic-terminated surface to a gallium-terminated surface with the methyl groups desorbing. The resulting gallium-terminated surface is no longer reactive with TMGa. A simple Lewis acid−base interaction between Ga and As would account for this selective chemisorption on arsenic sites. The problem with this selective adsorption mechanism is that theoretical[46] and experimental[47] evidence does not support this gallium-terminated surface. Gallium-rich surfaces all appear to have a significant fraction of As sites still exposed in the underlying layer. Consequently, ideal growth rates of 1 ML/reaction cycle cannot be explained during GaAs ALE.

Adsorbate inhibition is another proposed mechanism for GaAs ALE. In this model, the TMGa reacts with an arsenic-terminated surface and generates a gallium-rich surface covered with adsorbed methyl groups. The adsorbed methyl groups effectively inhibit further Ga deposition. This mechanism is supported by kinetic data for methyl radical desorption on gallium-rich surfaces.[48] The third widely cited mechanism is the flux balance mechanism that was originally proposed by Yu et al.[49] The key feature of the flux balance mechanism is that TMGa decomposes on a gallium-rich surface, and monomethylgallium or dimethylgallium (MMGa or DMGa) products quantitatively leave the surface and yield no net gallium deposition.[49] Creighton and co-workers have observed that gallium alkyl radicals desorb from a gallium-rich surface during their temperature programmed desorption studies.[50]

None of these mechanisms alone can explain all the experimental results for GaAs ALE. Strong evidence for the adsorbate inhibition mechanism comes from surface stability studies of methyl groups on the Ga-rich (4 × 6) GaAs(100) surface.[50,51] The most important result is that a new stable surface reconstruction occurs in the presence of adsorbed methyl groups that can stabilize a 1 ML coverage of Ga on the Ga-rich (4 × 6) surface.[51] In contrast, all previously observed Ga-rich surface reconstructions are terminated by a 0.75 ML Ga coverage. Gallium coverages greater than 0.75 ML are not detected by Auger or LEED above the methyl radical desorption temperature of 450 °C.[51] At these temperatures, the excess Ga forms droplets on the surface which can be observed under an optical microscope.[50] Consequently, the methyl groups appear to stabilize the Ga coverage at 1 ML and allow a pathway for ideal 1 ML/reaction cycle growth rates.

The reactions of $Ga(CH_3)_3$ and AsH_3 with GaAs have been studied extensively. Experimental evidence suggests that the TMGa reaction exhibits a zero-order TMGa pressure dependence,[9,10,43] even in the limit of excess gallium deposition. A zero-order dependence is a common feature of a surface unimolecular reaction mechanism.[50] The results indicate that, at high pressures ($>10^{-5}$ Torr) and typical ALE reaction temperatures (∼450−550 °C), the GaAs surface is saturated with adsorbed methyl groups. The reaction rate is determined solely by desorption of methyl radicals which explains the zero-order TMGa pressure dependence.

The As-rich surface has been shown to desorb methyl radical 10 times faster than a Ga-rich surface.[50] When TMGa reacts

with the As-rich surface, there is an initial rapid uptake of TMGa up to 1 ML followed by a slow, but finite, growth rate after the deposition of 1 ML of Ga. This change in adsorption rates explains the narrow operating window commonly observed for GaAs ALE.[9,10,50] Consequently, GaAs ALE can be viewed as driven by the difference in reaction rates of TMGa on the initial As-rich surface and the resultant Ga-rich surface. If the AsH_3 (B) half-reaction is initiated before TMGa can deposit excess Ga on the Ga-rich surface, then ALE behavior will be observed over a narrow set of pressure and exposure time parameters.

Unfortunately, the finite Ga deposition rates on the Ga-rich surface are in direct contrast with the results of Ozeki and Bedair.[43,52] The flux balance mechanism may help explain their observed wide 100 °C temperature window and near-ideal ALE behavior over a broad exposure range. From temperature programmed desorption experiments, monomethylgallium (MMGa) is known to desorb from the Ga-rich surface at ∼420 °C.[39,44] Ideal ALE behavior is predicted if MMGa comes off quantitatively after the deposition of 1 ML of Ga.

There are still discrepancies between various observations of GaAs ALE. For example, some studies observe a narrow ALE window indicative of excess Ga uptake, and others observe a broad ALE window. The explanation for these differences may be that the flux balance condition that occurs after the deposition of 1 ML of Ga is metastable.[39,44,53] Inhibiting the nucleation of Ga droplets is probably the key to producing near-ideal ALE behavior in the TMGa reaction. The conditions that favor Ga droplet formation are not well understood. Reactor design seems to be crucial in avoiding Ga droplet formation. Successful ALE behavior has been observed over a wide range of conditions in reactors that rapidly change the reactant gases. This procedure may minimize the heating of the thermal boundary layer and the gas phase pyrolysis of TMGa.[43,52]

The AsH_3 half-reaction is better understood than the TMGa reaction, but several issues must be addressed to explain the observed GaAs ALE. The As growth rate of 1 ML/reaction cycle over a wide pressure range can be explained by the known GaAs surface structures. The As-rich GaAs surface has a surface reconstruction of γ-(2 × 4) that is terminated with 1 ML of As.[51] This surface occurs at moderate AsH_3 exposures and is stable enough to survive the purge cycle. Most other As-rich surface reconstructions are terminated with 0.75 ML of As which is inconsistent with growth rates of 1 ML/reaction cycle. However, studies have shown that the most commonly observed As-rich c(2 × 8)/(2 × 4) surface reconstruction can be saturated with 1 ML of As in the presence of hydrogen adsorbates.[39] This stabilizing effect of hydrogen adsorbates for 1 ML of As is similar to the stabilizing effect of methyl adsorbates discussed earlier for 1 ML of Ga.

Another As-rich surface reconstruction that is sometimes observed is the c(4 × 4) surface.[50] This surface poses a problem for GaAs ALE because the c(4 × 4) surface is only as reactive toward TMGa as the Ga-rich surface. If this surface is formed, the disparity in rate constants between the As-rich and Ga-rich surfaces is lost, and GaAs ALE should not occur. Fortunately, this unreactive surface can be converted to a reactive As surface during a typical purge cycle under typical ALE reaction conditions. Consequently, all of the known As-rich surface reconstructions can account for growth rates of 1 ML/reaction cycle.

All the research in the surface chemistry of GaAs ALE has not led to the acceptance of a single mechanism. None of the proposed mechanisms can explain all of the experimental results, although a combination of the adsorbate inhibition and flux balance mechanisms seems the most plausible at this time. The surface chemistry does not follow the direct substitution reactions that are observed for SiO_2 and Al_2O_3 ALP and were originally proposed for GaAs ALE. Rather, the ALE window for GaAs deposition must be determined in a complicated way by the disparity in heterogeneous reaction rates toward the Ga-rich and As-rich surfaces.

C. Silicon and Germanium Atomic Layer Processing. The development of ALE approaches for the deposition of single elements has centered on silicon and germanium. This work has employed self-limiting surface reactions where the surface adsorbates produced during the reaction block reactive sites and limit the deposition. For example, diethylsilane will adsorb on clean silicon surfaces in the (A) half-reaction and deposit silicon, hydrogen, and ethyl groups at $T < 600$ K.[33,34] The hydrogen and ethyl groups will tie up silicon surface dangling bonds and eventually passivate the surface. These adsorbates can subsequently be removed by thermal annealing to $T > 700$ K in the (B) half-reaction.[33,34] The surface can then be cooled back down to $T < 600$ K, and more diethylsilane can be deposited to repeat the AB reaction cycle:

$$\text{(A)}\quad 2\text{Si}^* + \text{H}_2\text{Si}(\text{CH}_2\text{CH}_3)_2 \rightarrow \text{SiH}^* + \text{Si}-\text{SiH}(\text{CH}_2\text{CH}_3)_2{}^*$$

$$\text{(B)}\quad \text{SiH}^* + \text{Si}-\text{SiH}(\text{CH}_2\text{CH}_3)_2{}^* + \Delta T \rightarrow 3\text{Si}^* + 2\text{H}_2 + \text{CH}_2{=}\text{CH}_2$$

Similar strategies for germanium deposition have also been devised using diethylgermanium.[36−38,54,55]

Investigations have revealed that the silicon deposition is ∼0.13 ML per AB reaction cycle using this above approach with diethylsilane.[33,34,56] The submonolayer depositions are a consequence of the effective passivation by the surface adsorbates. Each molecular precursor deposits four ligands for every silicon atom in the diethylsilane molecule. Depositions of 1 ML will not be obtainable unless there are ways to remove the surface adsorbates during deposition. One possibility is electron stimulated desorption of hydrogen that could be employed to remove the hydrogen atoms that tie up the silicon dangling bonds.[57] Other schemes to remove the hydrogen could employ laser-induced thermal desorption.[58,59]

In addition to the nonthermal and laser methods to remove the surface adsorbates, chemical methods have also been devised for silicon ALE. These methods rely on the desorption kinetics of the reaction products resulting from the AB reaction. For example, chlorine does not desorb from silicon surfaces until $T > 950$ K, whereas HCl desorbs at $T \sim 750$ K and H_2 desorbs at $T \sim 700$ K.[60] Consequently, finite silicon coverages can be deposited on silicon surfaces at $T \sim 800$ K using Si_2Cl_6.[35] This (A) half-reaction will be limited by the chlorine coverage that will eventually passivate the surface. Subsequently, the surface can be exposed to Si_2H_6 in the (B) half-reaction, and additional silicon will deposit in conjunction with HCl desorption.[35] This (B) half-reaction is not self-limiting because H_2 can desorb at $T \sim 750$ K. However, if the Si_2H_6 exposure is limited in time, the disilane can act to deposit addition silicon and desorb the chlorine adsorbates in preparation for the next hexachlorodisilane exposure.

V. Film Deposition Using Binary Reaction Sequence Chemistry

Most studies of ALE and ALP have measured the thin film growth and have largely ignored the underlying surface chemistry. One system where both the surface chemistry and the growth rate have been determined is Al_2O_3 growth using the trimethylaluminum (TMA) and water precursors.[11,16,61] This section will compare the thin film growth rate and film

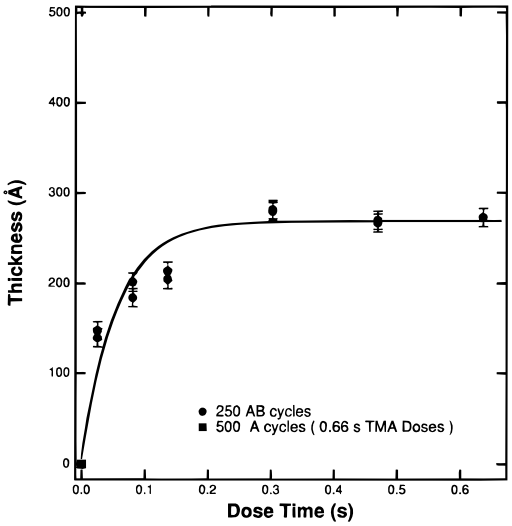

Figure 10. Thickness of Al_2O_3 films deposited on Si(100) after 250 AB cycles at 450 K versus (A) and (B) exposure time. The film thicknesses were measured using ellipsometry.

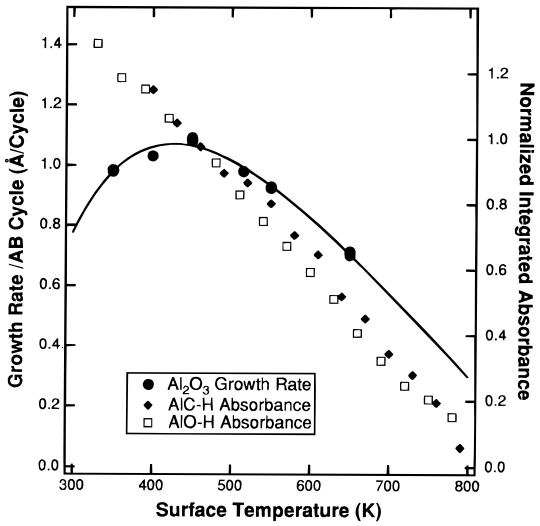

Figure 11. Al_2O_3 growth rate per AB reaction cycle as a function of surface temperature. These growth rates were determined by ellipsometry using Al_2O_3 film thicknesses measured after 250 AB reaction cycles. The thermal stabilities of the hydroxyl and methyl surface species are shown for comparison. These coverages were measured using the integrated absorbances of the AlO−H and AlC−H stretching vibrations.

roughness for Al_2O_3 ALP and demonstrate how these parameters are influenced by the surface chemistry.

A key characteristic of Al_2O_3 ALP is that each half-reaction in the binary reaction sequence goes to completion and reaches a saturation value. As a result, the Al_2O_3 growth rate is only dependent on the number of AB reaction cycles. The reaction conditions where the half-reactions reach saturation can be determined by varying the exposure time and monitoring the Al_2O_3 growth rate. Figure 10 shows the film thickness versus exposure time for Al_2O_3 growth using 250 AB cycles of TMA and H_2O on single-crystal Si(100) at 450 K.[11,61] The film thicknesses were measured in air using ellipsometry. The real index of refraction of the Al_2O_3 films was measured to be $n = 1.65$.

For exposure times less than 0.33 s, Figure 10 indicates that the film thickness after 250 AB cycles is very dependent on the exposure time.[11] This behavior is consistent with the (A) and (B) half-reactions not going to completion. For exposure times longer than 0.33 s, the growth rate of the film is independent of the exposure time. This observation indicates that the half-reactions are saturating at these conditions but does not necessarily imply that the half-reactions are going to completion.[11,61] However, the FTIR results shown in Figures 6−8 reveal that both reactions are indeed reaching completion at 500 K.[16]

The mechanism of Al_2O_3 ALP can also be tested by varying the surface temperature and measuring the growth rate/AB cycle. Figure 11 shows the Al_2O_3 growth rate versus surface temperature determined by measuring the film thickness after 250 AB cycles at various substrate temperatures.[61] At temperatures below 450 K, the growth rate increases with temperature. These results were obtained for exposures that were sufficient for the reactions to saturate, and increasing the exposure time further does not increase the growth rate. In agreement with the previous FTIR studies,[16] the lower Al_2O_3 growth rates at lower temperatures are consistent with half-reactions that do not go to completion at these lower temperatures.[16,61]

Figure 11 shows that the maximum Al_2O_3 growth rate is observed at 450 K.[11] The growth rate then decreases with increasing substrate temperature between 450 and 650 K. Similar measurements have been obtained for the Al_2O_3 growth rate versus surface temperature using TMA and hydrogen peroxide in a binary reaction sequence.[62] The decrease in the growth rate is closely correlated with the stability of the AlOH* and $AlCH_3$* surface species.[16,61]

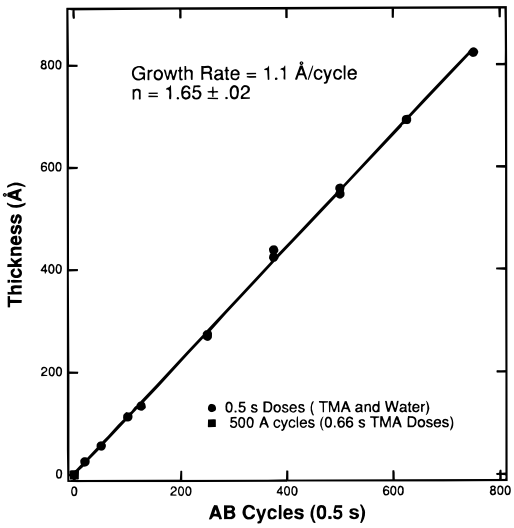

Figure 12. Thickness of Al_2O_3 films deposited on Si(100) versus number of AB reaction cycles performed with (A) and (B) exposure times of 0.5 s at 450 K.

The integrated infrared absorbances for the AlO−H and $AlC-H_3$ vibrational stretching modes versus temperature are also displayed in Figure 11. These measurements were performed on high surface area alumina membranes. The integrated absorbances were normalized relative to their values at 450 K. At higher surface temperatures, the AlOH* species are progressively lost by the dehydration reaction $2AlOH^* \rightarrow Al-O-Al + H_2O$,[16] whereas the $AlCH_3$* species may desorb as methyl radicals. The decreasing AlOH* and $AlCH_3$* surface coverages are in close correspondence with the decreasing Al_2O_3 growth rate. This correlation argues that the growth rate decreases concurrently with the number of reactive surface species. This behavior provides further evidence that the half-reactions are occurring through direct substitution reactions and the exchange of surface ligands.[61]

Figure 12 shows the Al_2O_3 film thickness versus the number of TMA/water AB cycles at 450 K.[11,61] These results reveal a linear growth rate of ~1.1 Å/AB cycle over the entire thickness range of the experiment. The growth rate of ~1.1 Å /AB reaction cycle indicates that this binary reaction sequence

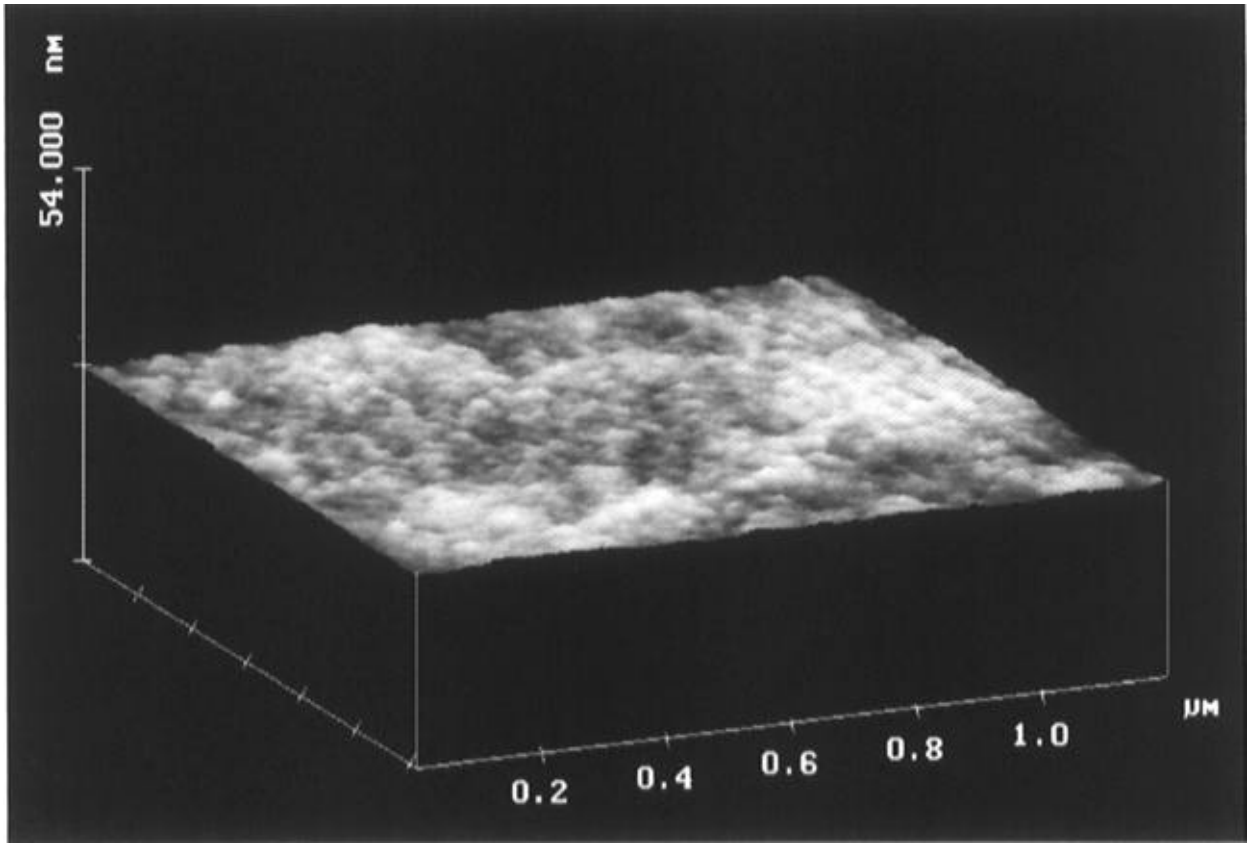

Figure 13. Atomic force microscope image of a Al_2O_3 film deposited on Si(100) after 250 AB cycles with (A) and (B) exposure times of 0.5 s at 450 K.

chemistry can be employed to deposit Al_2O_3 with atomic layer control. The growth rate is highly reproducible and can be utilized to deposit film thicknesses reliably to ±1 Å as determined by the ellipsometric measurements.

The real refractive index of the Al_2O_3 films determined by the ellipsometric measurements was $n = 1.65 \pm 0.02$. This index is consistent with a film density of $\rho = 3.5$ g/cm^3 using the Lorentz−Lorenz relationship.[61] This density is similar to densities of $\rho = 3.5-3.7$ g/cm^3 for the more open structure of γ-Al_2O_3 or amorphous alumina.[61] In comparison, the close-packed structure of α-Al_2O_3 has a higher density of $\rho = 3.97$ g/cm^3. The film density of $\rho = 3.5$ g/cm^3 is also in agreement with our earlier FTIR spectra of Al_2O_3 films on Si(100) that were consistent with amorphous Al_2O_3.[16]

The film density of $\rho = 3.5$ g/cm^3 can be utilized to estimate the film thickness corresponding to one Al_2O_3 monolayer. This density corresponds with a number density of $\rho = 2.07 \times 10^{22}$ Al_2O_3 units/cm^3. The thickness, d, of one Al_2O_3 monolayer can then be approximated using $d \sim \rho^{-1/3} = 3.64$ Å. The measured Al_2O_3 growth rate of ∼1.1 Å/AB reaction cycle at 450 K is much less than this estimated monolayer thickness.

Our earlier results for SiO_2 growth on Si(100) observed a SiO_2 deposition rate of ∼1.1 Å per AB reaction cycle at 600 K using $SiCl_4$ and H_2O in a binary reaction sequence.[17] This deposition rate was less than the estimated SiO_2 monolayer thickness of 3.5 Å.[17] This SiO_2 growth rate could be explained by the low SiOH* coverage of $\Theta_{OH} \sim 2.7 \times 10^{14}$ cm^{-2} resulting from dehydroxylation at the growth temperature of 600 K.[17] This hydroxyl coverage is ∼60% of the fully hydroxylated coverage of Θ_{OH} ∼4.6×10^{14} cm^{-2} at 300 K.[63]

For Al_2O_3, the AlOH* coverage at the growth temperature of 450 K is also reduced significantly compared with the saturation hydroxyl coverage observed at 300 K. On amorphous or γ-Al_2O_3 surfaces at 450 K, the AlOH* coverage is ∼70% of the fully hydroxylated coverage at 300 K.[16,64,65] On α-Al_2O_3 surfaces at 450 K, the AlOH* coverage may be as low as ∼25% of the fully hydroxylated coverage of $\Theta_{OH} \sim 1.5 \times 10^{15}$ cm^{-2} at 300 K.[66] Consequently, the submonolayer Al_2O_3 growth rates of ∼1.1 Å/AB reaction cycle at 450 K may be explained by the low thermal stability of the AlOH* surface species.

The linear Al_2O_3 growth rate observed in Figure 12 argues that the number of reactive surface sites must remain constant during the Al_2O_3 deposition. To confirm the constant surface area and evaluate the surface roughness, atomic force microscopy (AFM) measurements were performed in tapping mode on a Nanoscope III from Digital Instruments. The AFM images revealed that the Al_2O_3 films on Si(100) were extremely flat and uniform. Figure 13 shows an AFM image taken after 250 AB reaction cycles at 450 K.[11,61] The gray scale spans only 10 Å dark to light for this Al_2O_3 film that had a thickness of ∼270 Å.

The surface roughness of the Al_2O_3 ALP film is also independent of the number of AB reaction cycles. The power spectrum of the surface topography is shown in Figure 14.[61] The surface roughness is virtually indistinguishable for the original Si(100) substrate and the Al_2O_3 films deposited after various numbers of AB reaction cycles. These results for Al_2O_3 deposition are in marked contrast to the previous recent AFM results for TiO_2 ALP using $TiCl_4$ and H_2O in a binary reaction sequence.[12,14] In these studies, the deposited TiO_2 films were very rough, and the surface roughness changed with number of AB reaction cycles. This surface roughness for TiO_2 may indicate that the binary reaction conditions were not optimum. A detailed explanation of this surface roughness requires studies of the surface chemistry of TiO_2 ALP.

VI. Film Structure from Atomic Layer Controlled Growth

The structure of the films deposited by atomic layer controlled growth techniques is variable and depends on both the initial

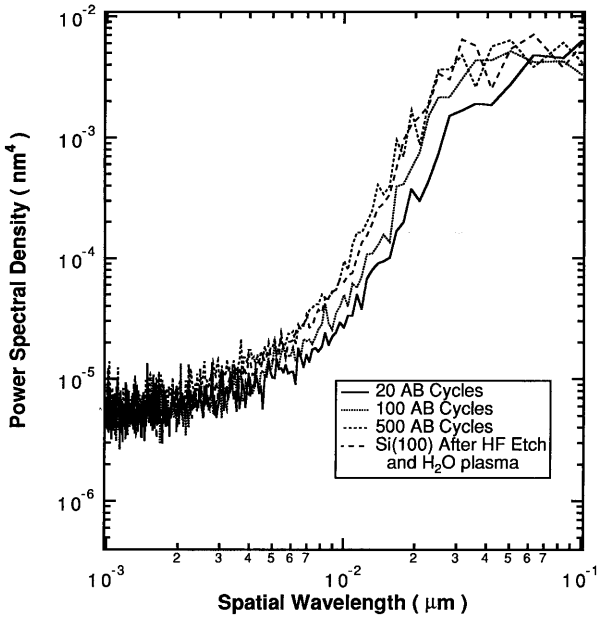

Figure 14. Power spectra of the surface topography of the Al_2O_3 film deposited on Si(100) versus number of AB reaction cycles. These power spectra were determined from the atomic force microscope images using 250 nm scan lengths.

substrate and the reaction temperature. Although ALE growth should be "epitaxial" by definition, the exact structure, orientation, and degree of crystallinity of the deposited film are not obvious. This uncertainty applies to both homoepitaxy and heteroepitaxy. Our lack of knowledge is particularly acute for the deposition of refractory oxide materials that may have a wide variety of structures ranging from amorphous to highly crystalline. In this section, we will concentrate on the recent work on Al_2O_3[23,61−65] and TiO_2[12,14] ALP.

Using the concepts of atomic layer processing, γ-Al_2O_3,[67] α-Al_2O_3,[68,69] and amorphous Al_2O_3[23,61] have been deposited on various substrates. The successful reports of growing crystalline α-Al_2O_3 films have all been performed at substrate temperatures greater than 450 °C.[67−69] These studies have concentrated on the film crystallinity and have not verified true atomic layer controlled growth. Crystalline α-Al_2O_3 films were first deposited by alternatingly dosing $AlCl_3$ and O_2 at various temperatures on sapphire and on Nb films epitaxially grown on sapphire.[68] Although the surface chemistry was not investigated, the most likely mechanism is that Al was deposited through the decomposition of $AlCl_3$ and was subsequently oxidized by the O_2 in the second dose. The crystallinity of the α-Al_2O_3 surface layers were monitored with reflection high-energy electron diffraction (RHEED).

Crystalline α-Al_2O_3 films were grown on the $(11\bar{2}0)$ and (0001) sapphire surface planes at temperatures above 600 °C.[68,69] In addition, a growth rate of ∼0.9 Å/cycle was observed that was consistent with less than one monolayer of Al_2O_3 deposited per cycle.[68] In the early stages of growth (10−30 cycles), the films appeared to become rougher. Later in film growth (∼150 cycles), the RHEED pattern of the film became streaky, indicating that the film was becoming smoother.[69] Similar results were observed on the Nb films, but crystalline α-Al_2O_3 films could be grown at lower temperatures of 450 °C. These studies showed that α-Al_2O_3 films can be grown on different types of substrates and at fairly high temperatures.

Another example of α-Al_2O_3 film deposition used TMA and either N_2O or H_2O_2 on Si(100).[62] Although these depositions were performed with no knowledge of the underlying surface chemistry, dense films with an index of refraction of $n = 1.75$ could be grown at substrate temperatures above 300 °C. At temperatures above 500 °C, the RHEED patterns indicated a polycrystalline structure when N_2O was used as the oxygen source. However, a growth rate of ∼10 Å/cycle was also observed at this temperature. This growth rate is not consistent with the expected growth rate of ≤1 ML/reaction cycle.

Transmission electron diffraction (TEM) have shown that Al_2O_3 films grown at $T = 100-450$ °C using the TMA/H_2O binary reaction sequence on Si(100) are amorphous. An upper limit of 10−15 Å was established for the crystalline sizes.[23] In addition, transmission FTIR spectra are also consistent with amorphous films grown at $T = 450$ K.[61] The low measured indices of refraction of $n = 1.64-1.70$ for these amorphous films were consistent with a film density less than crystalline sapphire. These studies suggest that crystalline films of α-Al_2O_3 can only be grown on crystalline substrates and at relatively high temperatures >800 K. Growth temperatures of $T > 650$ K are difficult for the TMA/H_2O reaction system because TMA pyrolyzes at $T \sim 650$ K.[31]

In addition to the successful growth of α-Al_2O_3 films, γ-Al_2O_3 films have also been grown on silicon substrates at temperatures >850 °C using a variant of ALP.[67] In this experiment, aluminum tri-*sec*-butoxide was pulsed into the chamber, and the molecule was allowed to decompose on the surface leaving behind Al_2O_3.[67] At temperatures above 850 °C, RHEED was used to confirm the γ-Al_2O_3 growth on both Si(100) and Si(110) surfaces. In contrast, crystalline films were not observed to grow on amorphous SiO_2 films. These results are intriguing because they demonstrate that more than one crystalline form of Al_2O_3 can be deposited using ALP techniques. Although these studies may not represent true ALP, they indicate that ALP concepts can be used to control the film structure in addition to growing conformal films with atomic layer controlled thicknesses.

In addition to crystalline Al_2O_3 film growth, the growth of crystalline TiO_2 films has also been reported using $TiCl_4$ and H_2O in a binary reaction sequence.[26,62] These experiments monitored the crystallinity of the TiO_2 films with X-ray diffraction (XRD). The attempts to deposit crystalline TiO_2 films on amorphous substrates were not successful.[26] However, both anatase and rutile TiO_2 structures were observed on single-crystal substrates.[26,62] The crystal structure was very dependent on the temperature and the substrate. In some instances, more than one crystal structure was observed in the same film.[26]

The idea of growing films with well-defined structure using ALP techniques has not received much attention. The recent results indicate that the structure of ALP films is sensitive to the substrate, substrate temperature, and even the particular molecular precursors. The few existing studies suggest that crystalline films can only be grown on crystalline substrates at relatively high temperatures. Polycrystalline films can also be deposited on amorphous substrates at high temperatures. This application of ALP is particularly important because thin passivating films of polycrystalline materials, such as α-Al_2O_3, are needed to protect materials used in harsh environments from corrosion.

VII. Complications during Binary Reaction Sequence Chemistry

Although the various models for binary reaction sequence chemistry appear to be quite straightforward, many complications can negate the elegance of the ALE approach. These complications can affect the interpretation of the underlying surface chemistry. These problems can also seriously alter the measured film growth rate and change the resulting surface morphology. This section will briefly discuss some of these complications and their effect on understanding the surface chemistry.

One of the most serious problems during binary reaction sequence chemistry is overlap of the pressures of the (A) and (B) molecular precursors. This overlap or "cross talk" can occur due to insufficient pumping or purging flow between the two half-reactions. As a result of this pressure overlap, the film growth will result from both ALP and chemical vapor deposition (CVD) contributions. The extra CVD portion of the film growth will significantly affect the interpretation of the film growth per AB reaction cycle in terms of self-limiting surface chemistry.

Because both ALP and CVD contributions yield the same film, determining the relative importance of "cross talk" is difficult. In general, the effect of the background pressure of the previous reactant can be determined by measuring the growth rate versus pumping time between the two half-reactions. If the growth rate is not changed by increasing the pump time, the "cross talk" is probably not a factor. Alternatively, the CVD kinetics for the binary reaction can be used to predict the film growth expected at the measured background pressures.

Another difficulty is optimizing the reaction conditions for the (A) and (B) half-reactions. The individual half-reactions may have different kinetics and different optimum pressure and temperature conditions.[20] The optimum conditions for the (A) half-reaction may be unsuitable for the (B) reaction, e.g. because of an unstable surface functional group. These separate optimum conditions will complicate studies of the surface chemistry at one set of pressures and surface temperature. Ideally, each half-reaction should be optimized individually. However, determining the best substrate temperature and reactant pressure for each half-reaction is difficult, and implementing different reaction conditions for each half-reaction is time-consuming for production reactors. Consequently, most film depositions are performed under conditions that represent a compromise for the two half-reactions.

Reactions on the walls of the reactor can also influence surface chemistry studies that monitor only the reactant products or measure only the total pressure in the reactor. In particular, much of the reactant may react with the walls before reaching the desired substrate if the half-reaction occurs at room temperature. Not only do these wall reactions waste reactant, they also can significantly affect total pressure measurements of the reactants. For example, the total pressure in the reactor may represent largely products because of wall reactions. Consequently, investigations of the pressure dependence of the surface chemical reaction kinetics may be seriously affected unless the partial pressures can be resolved with a mass spectrometer.

An additional complication is the effect of surface site inhomogeneities on binary reaction sequence chemistry. Ideally, the ALE approach would involve complete half-reactions where there is (1) a complete transition from one surface functional group to another in the direct substitution reaction model or (2) the growth of one complete elemental monolayer during each half-reaction in the model where the ligands on the element are lost during or shortly after the half-reaction. Because of inhomogeneities, the times required to go to completion during each half-reaction may be quite long. If the reaction times are shortened, deposition times may be reduced significantly, but then the interpretation of the surface chemistry must consider either both types of surface functional groups during each reaction for model 1 or reactions on a rougher surface consisting of several atomic layers for model 2.

Lastly, the interpretation of the surface chemistry can be affected by the high pressures in the viscous flow regime that are typically employed in the commercial ALE reactors that employ a carrier gas. With molecular precursors in viscous flow, the hot substrate may heat the carrier gas and activate the molecular precursor. The temperature dependence of the surface chemistry of a particular half-reaction then may reflect the thermal activation of the gas precursor instead of a thermally activated surface reaction. In particular, the kinetics for oxide growth using the ALP approach require high molecular precursor pressures in the viscous flow regime.[11,15−17] The kinetics for these reactions may likely be dependent on gas phase precursor activation as well as thermally activated surface reactions.

VIII. Conclusions and Future Prospects

The surface chemistry of atomic layer growth can be idealized in terms of self-limiting surface reactions. The basic model can be expressed by the binary reaction sequence approach for Al_2O_3 atomic layer processing using the trimethylaluminum ($Al(CH_3)_3$) and H_2O precursors:

$$\text{(A)}\quad AlOH^* + Al(CH_3)_3 \rightarrow Al{-}O{-}Al(CH_3)_2^* + CH_4$$

$$\text{(B)}\quad AlCH_3^* + H_2O \rightarrow AlOH^* + CH_4$$

In each half-reaction in the binary reaction sequence, the surface functionality is changed between a hydroxylated (AlOH*) surface to a methylated ($AlCH_3$*) surface, and vice versa. Each half-reaction goes to completion under the appropriate reaction conditions and is self-limiting. Consequently, the repetitive application of this ABAB... binary reaction sequence will deposit aluminum and oxygen in an atomic layer-by-layer controlled manner, and Al_2O_3 films are deposited at a rate of ∼1.1 Å/AB reaction cycle.

The atomic layer controlled deposition of Al_2O_3 and SiO_2 films is consistent with self-limiting, direct substitution, surface reactions. The atomic layer controlled deposition of GaAs is much more complicated and requires several surface chemical mechanisms to explain the observed 1 ML/AB reaction cycle growth rate. The complexity of GaAs ALE illustrates the need for further surface chemistry studies of atomic layer controlled growth. The underlying surface chemistry may dictate the film growth rate, film structure, and surface morphology. These surface chemistry studies are essential to understand and control the nanoscale fabrication methods that will be based on this binary reaction sequence chemistry approach.

There are numerous applications for atomic layer controlled film growth in microelectronics and optoelectronics. The SiO_2 gate dielectric in MOSFET devices is one obvious example where film thicknesses are currently approaching the tunneling limit at ∼10−15 atomic layer thicknesses. The deposition of higher dielectric gate oxide materials, such as TiO_2 or Al_2O_3, may quickly move to the forefront if various technological problems can be overcome. Other applications include the deposition of dielectric films on trench or stacked capacitors for DRAM high storage memory. In this case, the trench or stacked capacitor structure is not flat but has a very high aspect ratio. Conformal deposition on these structures, or other high aspect ratio porous materials, is not a problem for atomic layer controlled growth techniques. The self-limiting nature of the surface chemistry assures that deposition will be uniform as long as sufficient time is allowed for the surface reactions to reach completion.

Besides the ability to deposit conformally with atomic layer control in the vertical dimension, the binary reaction sequence approach can also be extended to the horizontal dimension in combination with other nanofabrication methods. For example, the surface functional groups dictate surface reactivity in the binary reaction sequence. If these functional groups are removed in some locations, the subsequent deposition can be

spatially localized to the pattern of the remaining functional groups. The surface functional groups also provide the chemical means to alternate between various materials with atomic layer control and form superlattice structures. This approach may provide new synthetic pathways to fabricate laminated structures and composite nanoscale materials.

As *The Journal of Physical Chemistry* looks ahead to its next 100 years, the names and topics will change, but our desire to understand and control the nanoscale world will remain. Atomic layer controlled growth will continue to be an integral part of nanofabrication methods. Many challenges and opportunities are on the horizon, and surface chemistry will continue to play a key role in the development of this area. The next 100 years should see spectacular advances in nanotechnology and the underlying surface chemistry that supports its foundations.

Acknowledgment. This work was supported by the Office of Naval Research under Grant N00014-92-J-1353. The Nanoscope III from Digital Instruments was obtained from an Instrumentation Grant from the National Science Foundation. The authors would like to thank Brenda R. Berens for her help typing and obtaining the references for this manuscript. We also acknowledge useful discussions with J. R. Creighton at Sandia National Laboratory.

References and Notes

(1) Chatterjee, P. K.; Graydon, G. B. *IEEE Trans. Syst.* **1993**, *1*, 7.
(2) Malhi, S.; Chatterjee, P. K. *IEEE Circ. Dev.* **1993**, *10*, 13.
(3) Masaki, A. *IEEE Circ. Dev.* **1992**, *8*, 18.
(4) Venkatesan, T. *Thin Solid Films* **1992**, *216*, 52.
(5) Goodman; C. H. L.; Pessa, M. V. *J. Appl. Phys.* **1986**, *60*, R65.
(6) Suntola, T.; Hyvarinen, J. *Annu. Rev. Mater. Sci.* **1985**, *15*, 177.
(7) Suntola, T. *Thin Solid Films* **1992**, *216*, 84.
(8) Pessa, M.; Makela, R.; Suntola, T. *Appl. Phys. Lett.* **1981**, *38*, 131.
(9) Nishizawa, J.; Hitoshi, A.; Kurabayashi, T. *J. Electrochem. Soc.* **1985**, *132*, 1197.
(10) Nishizawa, J.; Kurabayashi, T.; Abe, H. *Surf. Sci.* **1987**, *185*, 249.
(11) Ott, A. W.; McCarley, K. C.; Klaus, J. W.; Way, J. D.; George, S. M. *Appl. Surf. Sci.*, in press.
(12) Ritala, M.; Leskela, M.; Johansson, L. S.; Niinisto, L. *Thin Solid Films* **1993**, *228*, 32.
(13) Ritala, M.; Leskela, M. *Appl. Surf. Sci.* **1994**, *75*, 333.
(14) Kumagai, H.; Matsumoto, M.; Toyoda, K.; Obara, M.; Suzuki, M. *Thin Solid Films* **1995**, *263*, 47.
(15) George,S. M.; Sneh, O.; Dillon, A. C.; Wise, M. L.; Ott, A. W.; Okada, L. A.; Way, J. D. *Appl. Surf. Sci.* **1994**, *82*/*83*, 460.
(16) Dillon, A. C.; Ott, A. W.; Way, J. D.; George, S. M. *Surf. Sci.* **1995**, *322*, 230.
(17) Sneh, O.; Wise, M. L.; Ott, A. W.; Okada, L. A.; George, S. M. *Surf. Sci.* **1994**, *334*, 135.
(18) Niinisto, L.; Leskela, M. *Appl. Surf. Sci.* **1994**, *82*/*83*, 454.
(19) Lakomåå, E.-L.; Haukka; S.; Suntola, T. *Appl. Surf. Sci.* **1992**, *60*, 742.
(20) Emerson, R. M.; Hoyt, J. L.; Gibbons, J. F. *Appl. Phys. Lett.* **1994**, *65*, 1103.
(21) Khan, M. A.; Skogman, R. A.; Van Hove, J. M. *Appl. Phys. Lett.* **1990**, *56*, 1257.
(22) Khan, M. A.; Kuznia, J. N.; Olson, D. T. *Appl. Phys. Lett.* **1993**, *63*, 3470.
(23) Higashi, G. S.; Fleming, C. G. *Appl. Phys. Lett.* **1989**, *55*, 1963.
(24) Soto,C.; Tysoe, W. T. *J. Vac. Sci. Technol. A* **1991**, *9*, 2686.
(25) Viirola, H.; Niinisto, L. *Thin Solid Films* **1994**, *249*, 144.
(26) Ritala, M.; Leskela, M. *Thin Solid Films* **1993**, *25*, 288.
(27) Haukka, S.; Lakomaa, E.-L.; Suntola, T. *Thin Sol. Films* **1993**, *225*, 280.
(28) Asikainen, T.; Ritala, M.; Leskelo, M. *J. Electrochem. Soc.* **1994**, *141*, 3210.
(29) Ritala, M.; Leskela, M.; Niinisto, L.; Prohaska, T.; Friedbacher, G.; Grasserbauer, M. *Thin Solid Films* **1994**, *250*, 72.
(30) Dillon, A. C.; Ott, A. W.; Klaus, J. W.; George, J. M.
(31) Mayer, T. M.; Rogers, J. J. W.; Michalske, T. A. *Chem. Mat.* **1991**, *3*, 641.
(32) Asikainen, T.; Ritala, M.; Leskela, M. *Appl. Surf. Sci.* **1994**, *82*/*83*, 122.
(33) Coon, P. A.; Wise, M. L.; Dillon, A. C.; Robinson, M. B.; George, S. M. *J. Vac. Sci. Technol. B* **1992**, *10*, 221.
(34) Dillon, A. C.; Robinson, M. B.; Han, M. Y.; George, S. M. *J. Electrochem. Soc.* **1992**, *139*, 537.
(35) Gates, S. M.; Koleske, D. D.; Heath, J. R.; Copel, M. *Appl. Phys. Lett.* **1993**, *62*, 510.
(36) Takahashi, Y.; Sese, Y.; Urisu, T. *Jpn. J. Appl. Phys.* **1989**, *28*, 2387.
(37) Takahashi, Y.; Ishii, H.; Fujinaga, K. *J. Electrochem. Soc.* **1989**, *136*, 1826.
(38) Dillon, A. C.; Robinson. M. B.; George, S. M. *Surf. Sci. Lett.* **1993**, *286*, L535.
(39) Creighton, J. R.; Bansenauer, B. A. *Thin Solid Films* **1993**, *225*, 17.
(40) Heitzinger, J. M. White, J. M.; Ekerdt, J. G. *Surf. Sci.* **1994**, *299*/*300*, 892.
(41) Sneh, O.; George, S. M. *J. Vac. Sci. Technol.* **1995**, *A13*, 493.
(42) Ghandhi, S. K. *VLSI Fabrication Principles Silicon and Gallium Arsenide*; John Wiley and Sons: New York, 1983.
(43) Ozeki, M.; Ohtsuka, N.; Sakuma, Y.; Kodama, K. *J. Cryst. Growth* **1991**, *107*, 102.
(44) Yu, M. L.; Memmert, U.; Kuech, T. F. *Appl. Phys. Lett.* **1989**, *55*, 1011.
(45) Ozeki, M.; Mochizuki, K.; Ohtsuka, N.; Kodama, K. *Appl. Phys. Lett.* **1988**, *53*, 1509 (1988).
(46) Larsen, P. K.; Chadi, D. J. *Phys. Rev. B* **1988**, *37*, 8282.
(47) Duke, C. B. *J. Vac. Sci. Technol. B* **1993**, *11*, 1336 (1993).
(48) Creighton, J. R.; Lykke, K. R.; Shamamian, V. A.; Kay, B. D. *Appl. Phys. Lett.* **1990**, *57*, 279.
(49) Yu, M. L.; Memmert, U.; Buchan, N. I.; Kuech, T. F. In *Chemical Perspectives of Microelectronic Materials II*; Interannte, L. V., Jensen, K. S., Dubois,L. H., Gross, M. E., Eds.; Pittsburgh, PA, 1991; p 37.
(50) Creighton, J. R.; Banse, B. A. In *Materials Research Society Symposium Proceedings*; 1991; p 15.
(51) Creighton, R. J. *Appl. Surf. Sci.* **1994**, *82*/*83*, 171.
(52) Bedair, S. M.; El-Masry, N. A. *Appl. Surf. Sci.* **1994**, *82*/*83*, 7.
(53) Kobayashi, N.; Kobayashi, Y. *Thin Solid Films* **1993**, *225*, 32.
(54) Coon, P. A.; Wise, M. L.; George, S. M. *Surf. Sci.* **1992**, *278*, 383.
(55) Coon, P. A.; Wise, M. L.; Walker, Z. H.; George, S. M.; Roberts, D. A. *Appl. Phys. Lett.* **1992**, *60*, 2002.
(56) Coon, P. A.; Wise, M. L.; George, S. M. *J. Chem. Phys.* **1993**, *98*, 7485.
(57) Avouris, P.; Bozso, F.; Hamers, R. J. *J. Vac. Sci. Technol.* **1987**, *B5*, 1387.
(58) Koehler, B. G.; Mak, C. H.; Arthur, D. A.; Coon, P. A.; George, S. M. *J. Chem. Phys.* **1988**, *89*, 1709.
(59) Koehler, B. G.; George, S. M. *Surf. Sci.* **1991**, *248*, 158.
(60) Coon, P. A.; Gupta, P.; Wise, M. L.; George, S. M. *J. Vac. Sci. Technol.* **1992**, *A10*, 1992.
(61) Ott, A. W.; Klaus, J. W.; Johnson, J. M.; George, S. M. *Thin Solid Films*, in press.
(62) Kumagai, H.; Toyoda, K.; Matsumoto, M.; Obara, M. *Jpn. J. Appl. Phys.* **1993**, *32*, 6137.
(63) Sneh, O.; George, S. M. *J. Phys. Chem.* **1995**, *99*, 4639.
(64) Knozinger, H.; Ratnasamy, P. *Catal. Rev.—Sci. Eng.* **1978**, *17*, 31.
(65) Zamora, M.; Cordoba, A. *J. Phys. Chem.* **1978**, *82*, 584.
(66) Cameron, M. A.; Nelson, C. E.; Tolbert, M. A.; George, S. M. Manuscript in preparation.
(67) Iizuka, H.; Yokoo, L.; Ono, S. *Appl. Phys. Lett.* **1992**, *61*, 2978.
(68) Oya, G.; Yoshida, M.; Sawada, Y. *Appl. Phys. Lett.* **1987**, *51*, 1143.
(69) Oya G.; Sawada, Y. *J. Cryst. Growth* **1990**, *99*, 572.

JP9536763